Journal of Materials Chemistry A

Accepted Manuscript

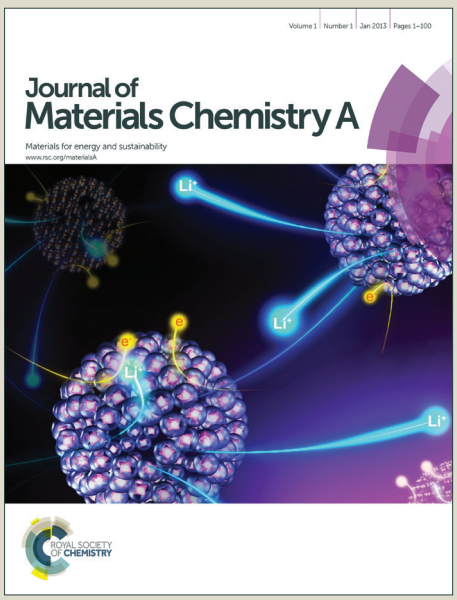

ROYAL SOCIETY OF CHEMISTRY

www.rsc.org/materialsA

Journal of Materials Chemistry A RSCPublishing

ARTICLE

$BaTiO_3$ Photoelectrodes for CdS Quantum Dot sensitized Solar Cells

Cite this: DOI: 10.1039/xoxxoooooox

Ke Meng, Praveen K. Surolia and K. Ravindranathan Thampi*,

Received ooth January 2012,
Accepted ooth January 2012

DOI: 10.1039/xoxxoooooox

www.rsc.org/

For the first time, layers of nano-sized perovskite $BaTiO_3$ particles were successfully applied as photoelectrodes for making CdS quantum dot sensitized solar cells (QDSSC). The optical and electrochemical properties of $BaTiO_3$ on FTO glass substrates were studied. The performance of cells was maximized by controlling the growth cycles of CdS and surface passivation of $BaTiO_3$ films. The encouraging power conversion efficiency (PCE) of 1.51% achieved points to the potential of using perovskites for sensitization and co-sensitization applications in third generation solar cells. It augers well with the recent trend of finding more compatible and stable perovskites for applications in mesoscopic sensitized solar cells.

Introduction

The third generation PV comprising of advanced thin films and newer PV concepts promise potentially higher energy conversion efficiencies and lower costs, among which dye- and Q-dot- sensitized solar cells (DSSC and QDSSC) are particularly promising[1]. QDSSCs have a particular advantage due to the beneficial optoelectronic properties of QDs[2]. It includes tuneable bandgaps, high molar extinction coefficients, large intrinsic dipole moments and scope for multiple charge carrier generation capabilities[3]. Semiconductor QDs of Cd-chalcogenides and PbS have been successfully applied as sensitizers in solar cells[4-7].

In a typical QDSSC, QDs are deposited on a wide band gap mesoporous semiconductor electrode film and typically TiO_2 is the most used electrode material[8, 9]. ZnO, SnO_2, Nb_3O_7 and Zn_2SnO_4, have also been studied as wide band gap semiconductor materials for Q-dot sensitization. Chen et al. applied single- and multi-layer porous ZnO nanosheets to make CdS QDSSC, which showed a maximum power conversion efficiency (PCE) of 1.16%[10]. SnO_2 was used as the wide band gap semiconductor material for CdS QDSSC by Zhou et al. while their cells resulted in a PCE of only 0.22%[11]. Zhang et al. used a highly crystalline Nb_3O_7F nanostructured photoelectrode in CdS QDSSC and achieved a PCE of 1.68%[12]. Zn_2SnO_4 nanorod arrays were introduced in CdS QDSSC by Bora et al. leading to a PCE of 1.24%[13]. Although the energy conversion performance of solar cells applying these wide band gap materials remain lower than that of cells applying TiO_2 nanostructures[14], various groups have investigated the effect of the wide band gap materials' optical and electrochemical properties on the photovoltaic performance of the solar cells[11-17] on the hope that better QDSSC could be developed in the near future using some of these highly stable wide bandgap oxides. Our report is a positive development in this direction.

Recently perovskite materials are intensively being studied in the realm of efficient third generation photovoltaic cells[18]. Perovskite like $CH_3NH_3PbI_3$ materials were employed as sensitizers in heterojunction solar cells providing power conversion efficiencies of over 15%[19, 20]. $(CH_3NH_3)PbI_3$ nanocrystals were also introduced as co-sensitizers in QDSSC yielding a power conversion efficiency of 6.5%[21]. There is also a study reporting perovskite materials as redox mediators from our group itself[22]. This recent trend to find replacements for traditional materials assumes significant importance for producing stable and reliable PV technologies even if the initial power conversion efficiencies are not record breaking. An all perovskite based stable solar cell is becoming a distinct possibility for which stable perovskites with good energy conversion efficiencies are required. Traditional perovskites of ABO_3 type are very stable and requires a revisit, especially where wide bandgap materials are suited for sensitization.

$BaTiO_3$ is a perovskite ferroelectric semiconductor with a band gap of 3.2 - 3.5 eV [23]. It was applied in the past as a wide band gap semiconductor for sensitization in DSSC; however, it was described as 'inert' due to its poor performance and the inability to bind dyes to the surface[24]. A thin $BaTiO_3$ layer was tested in QDSSC as a passivation layer for TiO_2 films in order to improve the cell performance by preventing charge recombination[25]. To the best of our knowledge, however, $BaTiO_3$ has not yet been successfully applied in QDSSC.

In this study, $BaTiO_3$ was introduced in QDSSC as a wide band gap semiconductor material for the first time. $BaTiO_3$ nanoparticles with diameters of tens of nanometres were synthesized first, followed by depositing it as meso-porous

School of Chemical and Bioprocess Engineering, University College Dublin, Belfield, Dublin 4, Ireland. *Fax: +35317161177; Tel: +35317161995; E-mail: ravindranathan.thampi@ucd.ie*

layers on FTO substrates via screen-printing. The obtained $BaTiO_3$ film was characterized to evaluate its electrical and optical properties. The $BaTiO_3$ films were then sensitized by CdS QDs to fabricate QDSSCs. The cells' performance was maximized by controlling the QDs growth cycles. Further cell performance improvement was obtained by passiviting the $BaTiO_3$ films with ZnO coating layers. An overall power conversion efficiency of 1.51% was obtained with V_{oc}=673 mV, J_{sc}=4.78 mA/cm^2 and FF=47.69% from our best cells. These results demonstrate that perovskite $BaTiO_3$ can be a promising photoelectrode material for QDSSCs and perhaps also for constructing an all perovskite stable novel PV cell allowing 15-20% PCE in the near future[26].

Experimental Section

Synthesis of $BaTiO_3$ nanoparticles: $BaTiO_3$ nanoparticles were synthesized through a hydrothermal method reacting $TiCl_4$ with $BaCl_2$ in a basic medium[27]. Typically, 5 ml of $TiCl_4$ (Aldrich) was added to 70 ml of chilled deionized (DI) water with stirring. 18 g of $BaCl_2{\cdot}2H_2O$ (Sigma) was then added to this solution while stirring. 150 ml of 2 M NaOH was further added to provide a basic pH. The final mixture was kept at 100°C for 8 hours in a round bottom flask equipped with a condenser for facilitating the $BaTiO_3$ crystal growth. The resulting precipitate was filtered and washed with DI water several times and dried in a furnace at 60°C.

Preparation of $BaTiO_3$ Photoelectrodes: The $BaTiO_3$ paste was prepared by following a standard procedure used to prepare TiO_2 paste[28]. Photoelectrodes were manufactured using the screen-printing method based on a layer-by-layer printing of $BaTiO_3$ paste on fluorine doped tin oxide (FTO) conducting transparent glass sheets. By controlling the number of prints, $BaTiO_3$ films with accurate thicknesses were fabricated. After this, the electrodes were sintered at 325°C, 375°C, 450°C and 500°C for 5 mins, 5 mins, 15 mins and 30 mins, respectively. The cell active area was 0.28 cm^2. A ZnO passivation layer on the $BaTiO_3$ films was manufactured by simply immersing the photoelectrode in 0.5 mM $Zn(NO_3)_2$ ethanol solution followed by air drying and sintering at 400°C for 30 min[29], when required. A TiO_2 passivation layer on the $BaTiO_3$ films was formed by dipping the photoelectrode in 50 mM $TiCl_4$ solution for 30 mins at 70°C, followed by rinsing and sintering at 500°C for 30 mins[30]. A $BaTiO_3$ passivation layer was deposited on the $BaTiO_3$ films by immersing the photoelectrode in 50 mM $BaCl_2$ and 50 mM $TiCl_4$ mixed solution for 10 mins, followed by 30 mins sintering at 400°C.

Sensitization of $BaTiO_3$ Films: The $BaTiO_3$ films were sensitized with CdS quantum dots using successive ionic absorption and reaction (SILAR) method. Briefly, 0.5 M $Cd(NO_3)_2$ ethanol solution and 0.5 M Na_2S methanol/DI water (1:1v) solution were prepared as the starting solutions for the SILAR process. The bare electrodes with $BaTiO_3$ layers were immersed into $Cd(NO_3)_2$ solution for 1 min at first, followed by 1 min rinsing by ethanol and 1 min drying by argon flow. The electrodes were then dipped into Na_2S solution for 1 min followed by further rinsing with methanol for 1 min and drying. Each series of the two dipping processes was called 'one SILAR cycle'. A ZnS passivation layer was always deposited on the CdS quantum dots by dipping the CdS sensitized electrodes alternately into 0.2 M Zn $(NO_3)_2$ in ethanol and 0.2 M Na_2S in methanol/DI water for 1 min/dip[9]. The electrodes were rinsed and dried with argon after each dipping.

Fabrication of QDSSC: A water based polysulfide electrolyte and Cu_2S counter electrodes were applied for fabricating cells. The electrolyte contains 1 M Na_2S, 1 M S and 0.1 M NaOH in DI water. The counter electrodes were fabricated following the procedure described in our earlier report[14]. Briefly, a Cu film with hundreds of nanometres thickness was firstly electrodeposited on FTO glass electrodes in a three-electrode system involving Ag/AgCl reference electrode, platinum wire counter electrode and an electrolyte of 5 mM $CuSO_4$, 1 M Na_2SO_4 and 0.5 M H_3BO_3 in deionized water. The Cu plated FTO glass piece was then immersed in a polysulfide solution containing 1 M Na_2S and 1M S in DI water for 1 min, followed by DI water rinsing and drying under argon flow. The working electrode and counter electrode were sandwiched together using a hot melt Bynel™ polymer gasket (50 micron thick). Electrolyte was filled into the space between the two electrodes through a hole in the counter electrode using vacuum back filling method. The back hole was finally sealed with a piece (0.1 mm thick) of glass heat sealed with Bynel™ polymer.

Characterization: Absorption and transmission spectra were recorded using a SPECORD 210 PLUS Double Beam UV-VIS spectrophotometer. XRD was measured using a Siemens D500 diffractionmeter. SEM images were recorded with a Hitachi TM-1000 Scanning Electron Microscope (SEM) (Hitachi High Technologies Ltd). EDX was carried out using an APOLLO XV Silicon Drift Detector and a Kratos Axis ULTRA was used to record the XPS spectra. Photoelectrochemical measurements including current density /voltage (J-V) curves, open circuit voltage (V_{oc}), short circuit current density (J_{sc}) and fill factor (FF) were measured using a Newport 91195A-1000 solar simulator and Newport 69920 Arc Lamp Power Supply. A Newport 81088A Air Mass Filter was placed before the output of the solar simulator to simulate the AM 1.5 spectrum with irradiance powers of 1000 W/m^2. J-V, electrochemical impedance spectroscopy (EIS) and open circuit voltage decay (OCVD) measurements were recorded with a GAMRY Instruments Potentiostat. Incident photon to current conversion efficiency (IPCE) was measured and recorded using a Gilden Photonics IPCE system and software.

Results and Discussion

The crystal structure and the nature of the as-prepared $BaTiO_3$ nanoparticles, $BaTiO_3$ films on FTO substrates and the CdS sensitized $BaTiO_3$ films on FTO substrates were characterized using X-ray diffractometry. Figure 1 (a) presents the XRD pattern of the as prepared $BaTiO_3$ powders. All the characteristic peaks were well indexed to the cubic phase of $BaTiO_3$ (JCPDS file No. 74-1968). The sharp peaks indicated the formation of well-crystalized, single phase $BaTiO_3$ crystal grains. Figure 1 (b) presents the XRD pattern of the $BaTiO_3$ films on FTO substrates. The newly emerged peaks were indexed to the FTO substrate (JCPDS file No. 77-0447). No separate peaks were observed after the CdS sensitization of the $BaTiO_3$ films coated FTO substrates as displayed in Figure 1 (c). The peaks of CdS are superimposed by both the $BaTiO_3$ and FTO peaks. However, the enhanced CdS coupled with $BaTiO_3$ or FTO peaks and weakened remaining peaks indicate the formation of CdS QDs, though with possible nano-sizes and lower crystallinity[31]

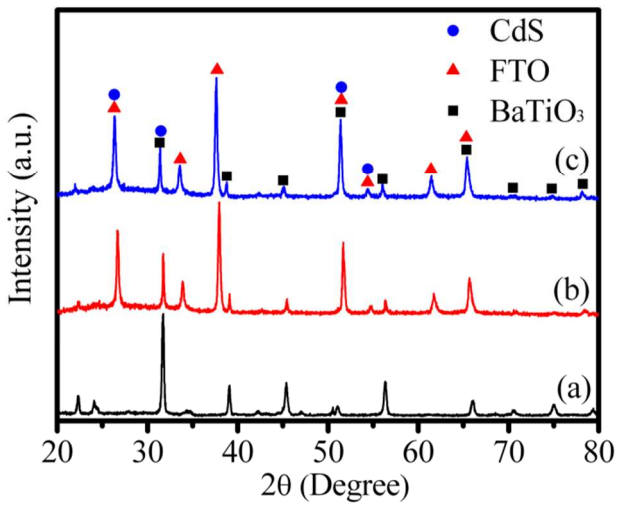

Figure 1: XRD patterns of the (a) $BaTiO_3$ nanoparticles (b) $BaTiO_3$ films on FTO substrates and (c) CdS sensitized $BaTiO_3$ films on FTO substrates

Scanning electron microscopy allowed investigation of the morphology of the $BaTiO_3$ nanoparticles and its films. Surface SEM image of $BaTiO_3$ nanoparticles shown in Figure 2 (a) and the particle-size distribution histograms seen in Figure 2 (b) indicate a narrow size distribution of the nanoparticles with an average diameter of around 34 nm, while the $BaTiO_3$ powders having an agglomerated shape and an aggregate size of 125-350 nm. Figure 2 (c) and (d) present surface and cross-section SEM The cross-section image (Figure 2 (d)) shows the porous structure of the $BaTiO_3$ film; while it also shows the resulting film is 26 µm in thickness. Figure 2 (e) and (f) show the surface and cross-section SEM of the CdS quantum dots sensitized $BaTiO_3$ films. Due to the small sizes of the QDs, no obvious difference was observed after the sensitization, however the remaining micro-size pores even after the CdS deposition allow an intimate contact between the electrolyte and the Q-dots, which enhances the regeneration of the QDs after electron injection and suppresses the charge recombination rate, thus improving the overall cell performance. The uniform coating of CdS QDs on $BaTiO_3$ film can be concluded from the EDX mapping on the cross section of the CdS sensitized $BaTiO_3$ films as shown in Figure 2 (g).

Light scattering ability of the wide band gap material in QDSSC is important for improving the light harvesting and thus the incident photon to current conversion efficiency (IPCE) of the cell[32]. UV-visible absorption and transmission spectroscopy was employed to characterize the light scattering ability of the $BaTiO_3$ films. According to Figure 3, the transmission of the $BaTiO_3$ films is only slightly higher than 20% in the visible range. The results indicate strongly the significant light scattering ability of the $BaTiO_3$ films. The scattering of light by spherical particles highly depends on the particle size and incident light wavelengths.[33] The $BaTiO_3$ nanoparticle aggregates with sizes of hundreds of nanometres have comparable size with the wavelength of visible light resulting in an enhanced light scattering. The multi-reflection between the $BaTiO_3$ particles can effectively enhance the optical pathway of incident light.

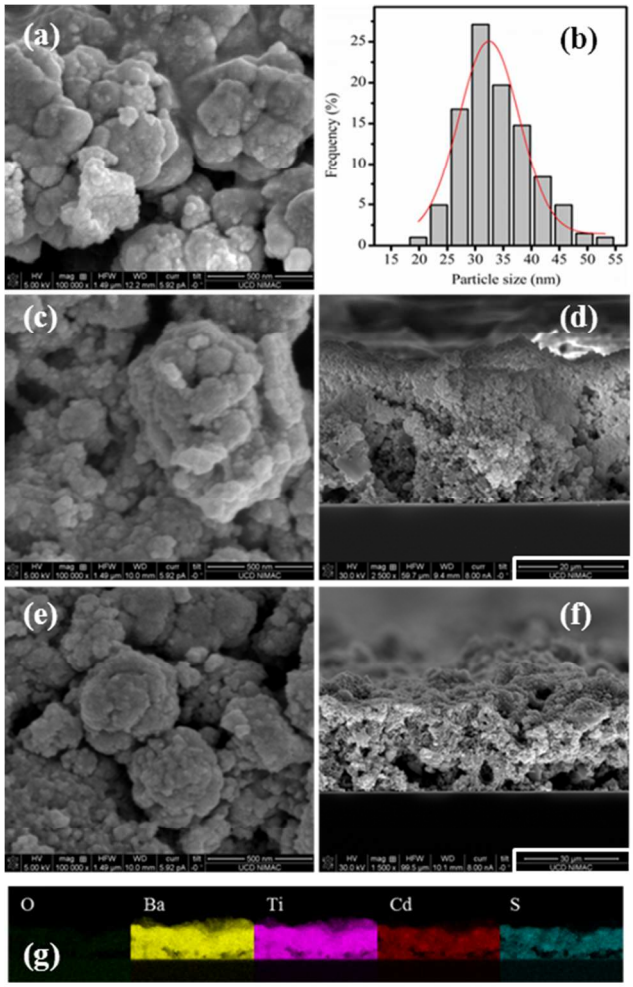

Figure 2: (a) Surface SEM image of $BaTiO_3$ nanoparticles (b) BaTiO3 particle-size distribution histograms (c) Surface SEM image of $BaTiO_3$ films on FTO (d) Cross-section SEM image of $BaTiO_3$ films on FTO (e) Surface SEM image of CdS sensitized $BaTiO_3$ films (f) Cross-section SEM image of CdS sensitized $BaTiO_3$ films on FTO (g) EDX mapping for the area shown by (f)

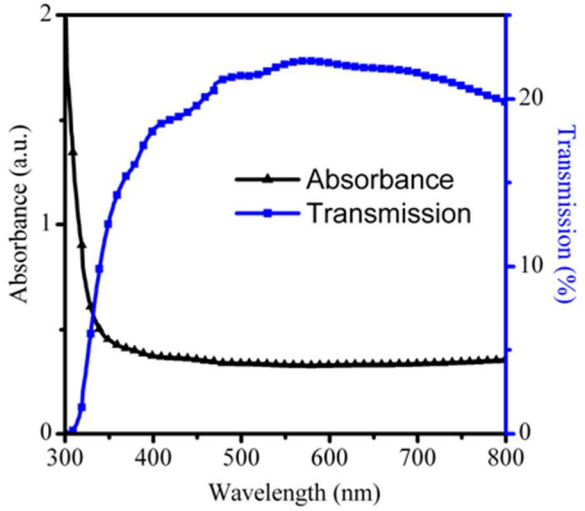

Figure 3: UV-visible absorption and transmission spectra of the $BaTiO_3$ films on FTO ($BaTiO_3$ film thickness 26 µm)

The energy level alignment between the wide band gap material and the sensitizer plays a vital role to construct efficient photovoltaics[34]. UV-vis absorption spectroscopy and X-ray photoelectron valance-band spectroscopy (XPS) determined the band edges of the $BaTiO_3$ nanoparticles. According to the UV-vis absorption spectrum of the $BaTiO_3$ films as shown in Figure 3, a band gap of 3.26 eV can be estimated for the $BaTiO_3$ nanoparticles. The XPS spectrum in Figure 4 (a) indicates the maximum valence band edge value is *ca.* 1.4 eV for the $BaTiO_3$ nanoparticles[35]. According to the energy diagram in Figure 4 (b), with similar band gap positions as TiO_2[36, 37], the $BaTiO_3$ nanoparticles should be a promising wide band gap material for CdS QDSSC due to the well matched band edges between CdS QDs and $BaTiO_3$ nanoparticles.

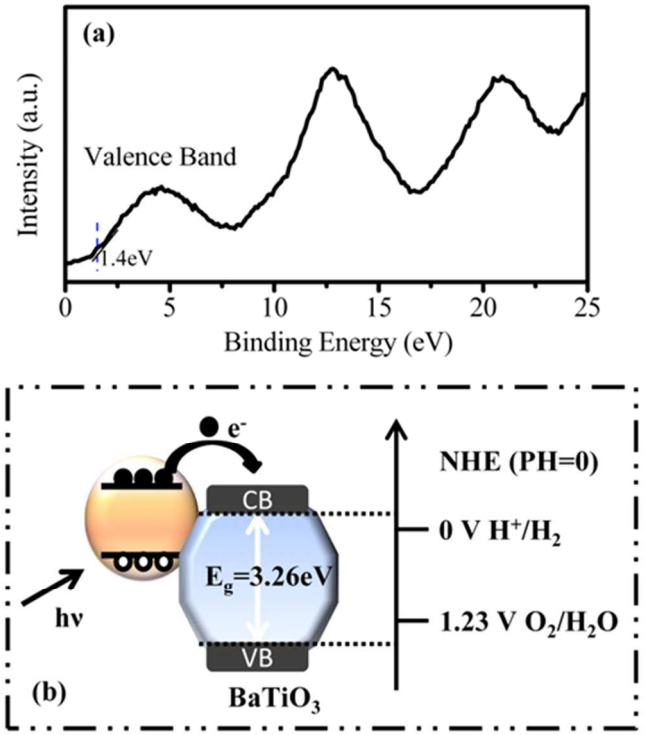

Figure 4: (a) XPS spectrum of the $BaTiO_3$ films (b) Energy alignment diagram of CdS-$BaTiO_3$ system

With the enhanced light scattering property and good band gap match, the $BaTiO_3$ nanoparticles could be considered as good wide band gap material for QDSSC. CdS quantum dots were deposited on $BaTiO_3$ films as sensitizers via SILAR method. 3-11 SILAR cycles of CdS were deposited on 26 µm $BaTiO_3$ films printed on FTO glass. The CdS quantum dots were always passivated with a ZnS thin layer. The J-V characteristics of solar cells are presented in Figure 5 and the cell parameters obtained from the J-V curves are listed in Table 1. The results show that with the increase of SILAR cycles from 3 to 9, the J_{sc} gradually increases from 1.04 to 3.79 mA/cm^2, which can be ascribed to additional SILAR cycles enhancing the deposition of bigger sizes and larger numbers of CdS quantum dots on $BaTiO_3$ films providing enhanced light absorption; while the V_{oc} increased from 491 to 608 mV and FF increased from 45.51 to 55.41%, which is due to the better coverage of CdS quantum dots on $BaTiO_3$ films. This reduces the charge recombination at the $BaTiO_3$/electrolyte interface. Further increase of CdS SILAR cycles to 11 leads to decreased J_{sc} of 3.36 mA/cm^2 and FF of 49.82%. This can be reasoned by the fact that after optimum deposition of CdS, too many SILAR cycles lead to more surface defects on the QDs, which increase the chances for charge recombination. Moreover, the overloaded CdS QDs may lead to pore blocking, which hinders the holes scavenging process. Thus, the optimized number of CdS SILAR cycles on 26 µm $BaTiO_3$ films is obtained at 9 cycles with a power conversion efficiency (PCE) of 1.26%. The thickness of $BaTiO_3$ films was also varied by controlling the number of $BaTiO_3$ layers on FTO substrate to maximize the cell performance. Solar cells with 3, 5, 7 and 9 layers of $BaTiO_3$ sensitized by 9 cycles of CdS were fabricated and cells with 7 layers of $BaTiO_3$ showed the best performance. The 7 layers $BaTiO_3$ film has a thickness of 26 µm and it is taken for all other film characterizations.

As discussed in the introduction part, an earlier study[24], which used $BaTiO_3$ nanoparticles based photoelectrodes for DSSC applications, have described this material as 'inert' when interacted with dyes. However, in cells where they decorated the 50 nm diameter $BaTiO_3$ particles with 5 nm TiO_2 nanoparticles, a promising overall power conversion efficiency of more than 5% was measured. They attributed the low performance of the $BaTiO_3$/dye system to the poor affinity of dye on $BaTiO_3$ particles, and by introducing a network of TiO_2 particles the dye adsorption was greatly enhanced. This resulted in enhanced photocurrents and higher photo conversion efficiencies[24]. Indeed, the interaction between dye and TiO_2 is mainly attributed to the affinity between the carboxylic anchoring-group of the dye and the Ti^{4+} ions on the TiO_2 (101) plane[38]. When Ba^{2+} ions are introduced through the crystalline $BaTiO_3$ into such a semiconductor system, the bonding affinity and electronic coupling between the dye and the titanium ions in the $BaTiO_3$ could be weakened. However, in the $BaTiO_3$/CdS QD case, the CdS quantum dots are crystalized and grown directly on the $BaTiO_3$ particles without any anchoring –COOH group. The situation with respect to its affinity to $BaTiO_3$ and its electron injection ability are considerably different. Thus the promising performance of CdS quantum dot sensitized $BaTiO_3$ solar cells is made possible[3].

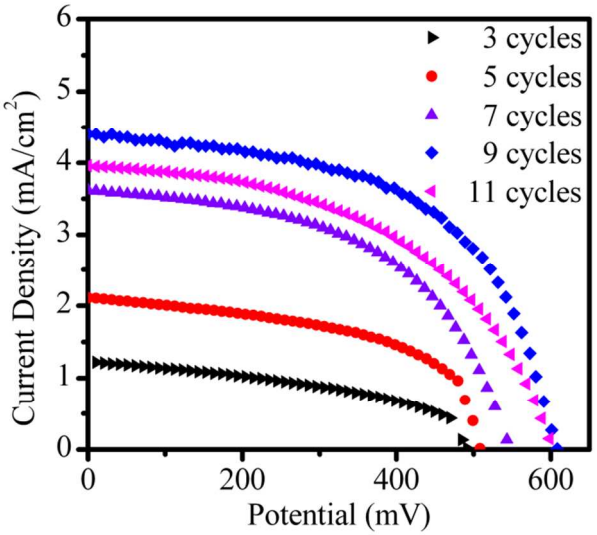

Figure 5: J-V characteristic of cells applying different numbers of SILAR cycles on $BaTiO_3$ films

Table 1 Cell performance parameters obtained from J-V measurements of the cells applying different numbers of SILAR cycles

Cycles	V_{oc} (mV)	J_{sc} (mA/cm^2)	FF (%)	η (%)
3	491	1.04	45.51	0.24
5	508	1.79	54.32	0.50
7	543	3.07	53.64	0.89
9	608	3.74	55.41	1.26
11	606	3.36	49.82	1.00

UV-vis absorption spectra of the CdS QDs sensitized $BaTiO_3$ photoelectrodes were recorded to evaluate the sizes and numbers of the incorporated CdS QDs and are presented in Figure 6 (a). The absorbance increases with increasing SILAR cycles indicating the increased amount of CdS QDs deposition, while the growth of the CdS QD size is suggested by the red shift of the absorbance shoulder and onset position[39]. Figure 6 (b) shows the incident photon to current conversion efficiency (IPCE) of cells fabricated with 9 cycles of CdS deposition on $BaTiO_3$ films. A maximum IPCE of 30% was obtained at 400 nm. The IPCE values were integrated with the incident photon flux of standard AM1.5 to get the calculated $J_{sc,}$ which is 2.83 mA/cm^2. The measured J_{sc} value of 3.74 mA/cm^2 as shown in Table 1 is slightly higher than the calculated value, which is due to fact that charge separation and collections are more efficient under a much higher illumination intensity (J-V measurement) than that used for the IPCE measurement[40].

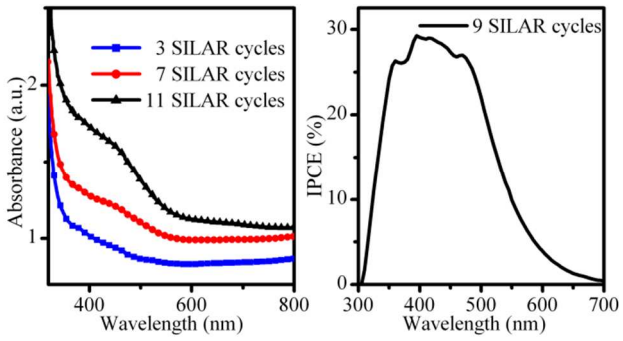

Figure 6: (a) UV-vis absorption spectra of $BaTiO_3$ films applying different numbers of SILAR cycles (b) IPCE curve of the cells with 9 CdS SILAR cycles on $BaTiO_3$ films

In an effort to enhance the electron transfer from QDs to $BaTiO_3$ and suppress the back electron transfer at the electrode-electrolyte interface, different passivation layers were introduced on the $BaTiO_3$ films. All the cells with different passivation layers on $BaTiO_3$ films contained 9 SILAR cycles of CdS deposition. The performance parameters of the cells with different coating layers are listed in Table 2. Single or double passivation layers were deposited on the $BaTiO_3$ films. As shown in Table 2, the different passivation strategies have different effects on the cell performance; single ZnO or TiO_2 coating layer enhances the cell performance while the double TiO_2, TiO_2+ZnO or $BaTiO_3$ coating layers suppress cells' over all power conversion efficiencies. Among all the coating strategies employed, cells with ZnO coating layer show optimized power conversion efficiencies. Hence, further studies were taken on cells applying ZnO passivation layers. Solar cells applying bare ZnO films consisting of ZnO nanoparticles synthesized using procedures reported in literature[41] were also fabricated for comparison. The relevant cell performance parameters are listed in Table 2. The measured PCE of cell applying bare ZnO photoelectrode is 0.57%, which is mainly restricted by the low fill factor of 23.03%. This may be blamed on the surface defects present on the ZnO nanoparticles.

Table 2 Performance parameters of the cells fabricated with different passivation strategies

Coating layers	V_{oc} (mV)	J_{sc} (mA/cm^2)	FF (%)	η (%)
Bare $BaTiO_3$	608	3.74	56.18	1.26
Bare ZnO	473	5.25	23.03	0.57
ZnO	673	4.78	47.69	1.51
TiO_2	550	4.20	60.09	1.39
Double TiO_2 layer	465	3.35	44.71	0.70
TiO_2+ZnO	539	4.09	55.87	1.23
$BaTiO_3$ layer	630	3.02	45.50	0.87

The J-V characteristics and cells parameters with and without the ZnO passivation layers on $BaTiO_3$ films are shown in Figure 7 and Table 2, respectively. With introduction of the ZnO passivation layer, the V_{oc} of the cells have increased significantly from 608 mV to 673 mV. V_{oc} is determined by the difference between the quasi-Fermi level of the photoelectrode and the redox potential of the electrolyte; it is also dependent on the rate of the electron recombination at the semiconductor-electrolyte interface[42]. The introduction of ZnO with its high conduction band edge helps to increases the quasi-Fermi level of the photoelectrode while the compact ZnO layer itself operates as an energy barrier to the back electron transfer from $BaTiO_3$ nanoparticles to the electrolyte. Both of these contribute to the higher V_{oc}. The J_{sc} of the cells applying ZnO passivation layer also increases by 1 mA/cm^2, which further suggests the suppression of electron recombination occurring at the $BaTiO_3$-electrolyte interface. Overall, the cells with ZnO passivation layer show a promising power conversion efficiency of 1.51%, which is 20% higher than cells with bare $BaTiO_3$ films sensitized by CdS QDs.

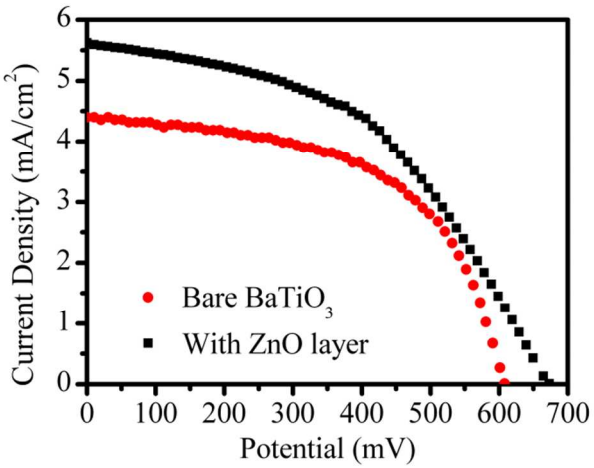

Figure 7: J-V characteristics of cells with and without ZnO coating layer on $BaTiO_3$ films

Electrochemical impedance spectroscopy (EIS) was introduced to investigate the impact of the ZnO passivation layer on the cell performance. Figure 8 (a) shows typical Nyquist plots of the cells with and without the ZnO coating layer. A typical EIS spectrum of DSSC consists of three semicircles responding to the high-frequency, middle-frequency and low-frequency regions when the cells are biased at its V_{oc}; while the responses are attributed to the charge transfer at the counter electrode-electrolyte interface, the carrier transport at the photoanode-electrolyte interface and the ions diffusion process in the electrolyte, correspondingly[43]. This characteristic is also applicable to QDSSC except that for a relatively low-performing QDSSC, a double-semicircle spectrum is always observed where the feature of the diffusion process is not presented[44-46]. In this study, we focus on the charge transfer and recombination at the $BaTiO_3$/electrolyte interface in the middle-frequency region. Nyquist plots of both cells indicate the ZnO layer reduces the charge transfer resistance, which is mainly due to the suppression of charge recombination at the $BaTiO_3$/electrolyte interface. The Bode-phase plots of the cells obtained from EIS measurement (Figure 8 (b)) were introduced to investigate the electron life time (τ_n) in the CdS sensitized $BaTiO_3$ nanostructure using the equation $\tau_n=1/(2\pi f_{max})$ where f_{max} is the maximum frequency of the middle-frequency peak[47]. The f_{max} values for cells with and without ZnO layer are 30 Hz and 63 Hz, respectively. Correspondingly, the electron lifetime is calculated to be 5.3 ms and 2.5 ms for the cells assembled by $BaTiO_3$ films with ZnO coating layer and bare $BaTiO_3$ films, respectively. The longer electron lifetime by introduction of the ZnO layer demonstrates the retardation of charge recombination at the $BaTiO_3$ /electrolyte interface.

Open circuit voltage decay measurements (OCVD) helped to further analyse the excited electron lifetimes[48]. The results in Figure 9 indicate that the V_{oc} decay of cells with ZnO coating layer is much slower than cells with bare $BaTiO_3$. Lower V_{oc} decay leads to increase in the electron life time. This further indicates the ZnO layer's ability to suppress electron recombination at the $BaTiO_3$-electrolyte interface. The results obtained from OCVD are consistent with the results acquired from the EIS measurements. We conclude that ZnO coating on $BaTiO_3$ films can therefore effectively suppress electron leakage and thus enhance the overall cell performance.

Figure 10 is a schematic illustration of the effect of ZnO passivation layer on $BaTiO_3$ films. The electron recombination is suppressed by the coating of the ZnO layer. As per the proposed mechanism, excited electrons in the conduction band of CdS can effectively inject into the conduction band of $BaTiO_3$ through the ZnO intermediate energy level; however, the ZnO layer works as an energy barrier prohibiting the back electron transfer from the conduction band of $BaTiO_3$ into the electrolyte. As a result, the number of electrons injected to the FTO substrate increases leading to a higher J_{sc} while the electron accumulation in the $BaTiO_3$ is also enhanced resulting in a high V_{oc}, thereby the overall power conversion efficiency is improved.

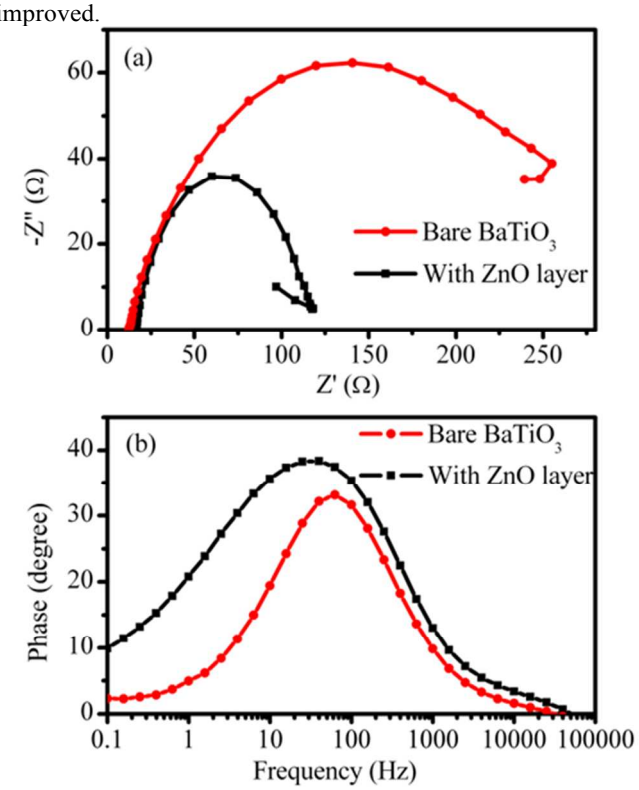

Figure 8: (a) Nyquist plots and (b) Bode-phase plots of cells with and without ZnO coating layers on $BaTiO_3$ films. (Cells measured under 1 sun at $V=V_{oc}$)

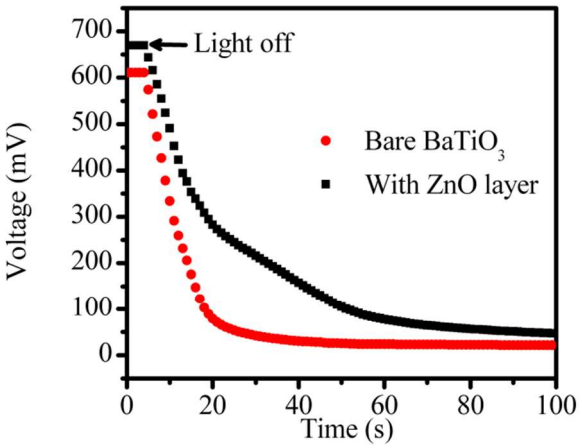

Figure 9: OCVD curves of cells with and without ZnO coating layer on $BaTiO_3$ films.

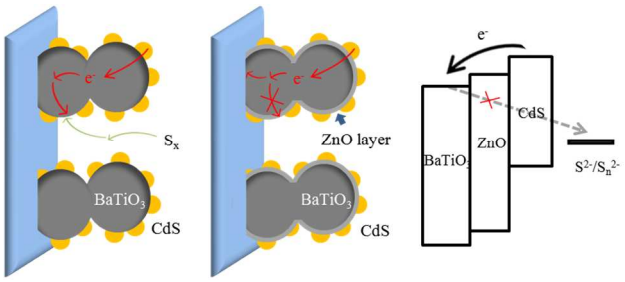

Figure 10: Schematic figures of CdS/bare $BaTiO_3$ system (left), CdS/ZnO layer/$BaTiO_3$ system (middle) and energy diagram at photoelectrode/electrolyte interface (right)

Conclusions

$BaTiO_3$ nanoparticles were synthesized and characterized to investigate their optical and electrical properties. The nanoparticles were further introduced successfully as a wide band gap material in QDSSC, which to the best of our knowledge, is for the first time. Sensitized by CdS QDs via SILAR method, the QDSSC applying the $BaTiO_3$ films showed maximum power conversion efficiencies at 9 SILAR cycles. A ZnO coating layer was then applied on $BaTiO_3$ films and a PCE of 1.51% was obtained which is 20% higher than cells with bare $BaTiO_3$ films. The enhancement of cell performance is attributed to the suppression of back electron transfer at the $BaTiO_3$-electrolyte interface by the ZnO passivation layer, which was ascertained by EIS and OCVD measurements. The results indicate that the perovskite type $BaTiO_3$ material is indeed a promising wide band gap material for third generation solar cells such as QDSSC. This is to be seen in the light of the recent advancements made in solar cells using perovskites.

Acknowledgements

Ke Meng acknowledges the funding support received from China Scholarship Council. Praveen K. Surolia received support from European Commission's FP7 SMARTOP project under the Grant Agreement number 265769. K.R. Thampi acknowledges the SFI-Airtricity Stokes professorship grant.

Notes and references

1. A. Yella, H.-W. Lee, H. N. Tsao, C. Yi, A. K. Chandiran, M. K. Nazeeruddin, E. W.-G. Diau, C.-Y. Yeh, S. M. Zakeeruddin and M. Grätzel, *Science*, 2011, 334, 629-634.
2. P. V. Kamat, *The Journal of Physical Chemistry C*, 2008, 112, 18737-18753.
3. I. Mora-Seró, S. Giménez, F. Fabregat-Santiago, R. Gómez, Q. Shen, T. Toyoda and J. Bisquert, *Accounts of chemical research*, 2009, 42, 1848-1857.
4. P. K. Santra and P. V. Kamat, *Journal of the American Chemical Society*, 2012.
5. J.-W. Lee, D.-Y. Son, T. K. Ahn, H.-W. Shin, I. Y. Kim, S.-J. Hwang, M. J. Ko, S. Sul, H. Han and N.-G. Park, *Scientific Reports*, 2013, 3.
6. Z. Yang and H. T. Chang, *Solar Energy Materials and Solar Cells*, 2010, 94, 2046-2051.
7. S. D. Sung, I. Lim, P. Kang, C. Lee and W. I. Lee, *Chemical Communications*, 2013, 49, 6054-6056.
8. H. Jun, M. Careem and A. Arof, *Renewable and Sustainable Energy Reviews*, 2013, 22, 148-167.
9. X.-Y. Yu, B.-X. Lei, D.-B. Kuang and C.-Y. Su, *Journal of Materials Chemistry*, 2012, 12058-12063.
10. H. Chen, W. Li, H. Liu and L. Zhu, *Electrochemistry Communications*, 2011, 13, 331-334.
11. X. Zhou, W. Fu, H. Yang, Y. Li, Y. Chen, M. Sun, J. Ma, L. Yang, B. Zhao and L. Tian, *Electrochimica acta*, 2013, 89, 510-515.
12. H. Zhang, Y. Li, Y. Wang, P. Liu, H. Yang, X. Yao, T. An, B. Wood and H. Zhao, *Journal of Materials Chemistry A*, 2013, 1, 6563-6571.
13. T. Bora, H. H. Kyaw and J. Dutta, *Electrochimica acta*, 2012, 68, 141-145.
14. K. Meng, P. K. Surolia, O. Byrne and K. R. Thampi, *J Power Sources*, 2014, 248, 218-223.
15. J. Jean, S. Chang, P. R. Brown, J. J. Cheng, P. H. Rekemeyer, M. G. Bawendi, S. Gradečak and V. Bulović, *Advanced Materials*, 2013.
16. M. A. Hossain, Z. Y. Koh and Q. Wang, *Physical Chemistry Chemical Physics*, 2012.
17. L.-B. Li, Y.-F. Wang, H.-S. Rao, W.-Q. Wu, K.-N. Li, C.-Y. Su and D.-B. Kuang, *ACS Applied Materials & Interfaces*, 2013, 5, 11865-11871.
18. G. Hodes, *Science*, 2013, 342, 317-318.
19. J. H. Heo, S. H. Im, J. H. Noh, T. N. Mandal, C. S. Lim, J. A. Chang, Y. H. Lee, H. J. Kim, A. Sarkar, M. K. Nazeeruddin, M. Gratzel and S. I. Seok, *Nature photonics*, 2013, 7, 487-492.
20. M. Liu, M. B. Johnston and H. J. Snaith, *Nature*, 2013, 501, 395-398.
21. J.-H. Im, C.-R. Lee, J.-W. Lee, S.-W. Park and N.-G. Park, *Nanoscale*, 2011, 3, 4088-4093.
22. J. R. Kantor, 1924.
23. S. O'Brien, L. Brus and C. B. Murray, *Journal of the American Chemical Society*, 2001, 123, 12085-12086.
24. M. Zhong, J. Shi, W. Zhang, H. Han and C. Li, *Materials Science and Engineering: B*, 2011, 176, 1115-1122.
25. S.-K. Kim, M.-K. Son, S. Park, M.-S. Jeong, K. Prabakar and H.-J. Kim, *Electrochimica acta*, 2014, 118, 118-123.
26. N.-G. Park, *The Journal of Physical Chemistry Letters*, 2013, 4, 2423-2429.
27. Y. Gao, V. V. Shvartsman, A. Elsukova and D. C. Lupascu, *Journal of Materials Chemistry*, 2012, 22, 17573-17583.
28. S. Ito, P. Chen, P. Comte, M. K. Nazeeruddin, P. Liska, P. Pechy and M. Grätzel, *Progress in photovoltaics: research and applications*, 2007, 15, 603-612.
29. S. Ameen, M. S. Akhtar, H. K. Seo and H. S. Shin, *Advanced Energy Materials*, 105-166.
30. N. Fuke, R. Katoh, A. Islam, M. Kasuya, A. Furube, A. Fukui, Y. Chiba, R. Komiya, R. Yamanaka and L. Han, *Energy & Environmental Science*, 2009, 2, 1205-1209.
31. H. Cheng, X. Zhao, X. Sui, Y. Xiong and J. Zhao, *Journal of Nanoparticle Research*, 2011, 13, 555-562.
32. X. Song, M. Wang, T. Xing, J. Deng, J. Ding, Z. Yang and X. Zhang, *J Power Sources*, 2014, 253, 17-26.
33. S. Hore, P. Nitz, C. Vetter, C. Prahl, M. Niggemann and R. Kern, *Chemical Communications*, 2005, 2011-2013.
34. D. R. Baker and P. V. Kamat, *Advanced Functional Materials*, 2009, 19, 805-811.

35. X. Chen, L. Liu, Y. Y. Peter and S. S. Mao, *Science*, 2011, 331, 746-750.
36. H. Zhang, X. Liu, Y. Li, Q. Sun, Y. Wang, B. J. Wood, P. Liu, D. Yang and H. Zhao, *Journal of Materials Chemistry*, 2012, 22, 2465-2472.
37. J. Pan, G. Liu, G. Q. M. Lu and H. M. Cheng, *Angewandte Chemie International Edition*, 2011, 50, 2133-2137.
38. K. E. Lee, M. A. Gomez, T. Regier, Y. Hu and G. P. Demopoulos, *The Journal of Physical Chemistry C*, 2011, 115, 5692-5707.
39. Y. L. Lee and Y. S. Lo, *Advanced Functional Materials*, 2009, 19, 604-609.
40. G. P. Smestad, F. C. Krebs, C. M. Lampert, C. G. Granqvist, K. Chopra, X. Mathew and H. Takakura, *Solar Energy Materials and Solar Cells*, 2008, 92, 371-373.
41. K. K. Wong, A. Ng, X. Y. Chen, Y. H. Ng, Y. H. Leung, K. H. Ho, A. B. Djurišić, A. M. C. Ng, W. K. Chan and L. Yu, *ACS Applied Materials & Interfaces*, 2012, 4, 1254-1261.
42. P. Sudhagar, T. Song, D. H. Lee, I. Mora-Seró, J. Bisquert, M. Laudenslager, W. M. Sigmund, W. I. Park, U. Paik and Y. S. Kang, *The Journal of Physical Chemistry Letters*, 2011, 2, 1984-1990.
43. Y. Bai, H. Yu, Z. Li, R. Amal, G. Q. M. Lu and L. Wang, *Advanced Materials*, 2012, 24, 5850-5856.
44. H. K. Jun, M. A. Careem and A. K. Arof, *Nanoscale research letters*, 2014, 9, 1-7.
45. M.-H. Yeh, L.-Y. Lin, C.-P. Lee, C.-Y. Chou, K.-W. Tsai, J.-. Lin and K.-C. Ho, *J Power Sources*, 2013, 237, 141-148.
46. J. Kim, H. Choi, C. Nahm, C. Kim, S. Nam, S. Kang, D. R. Jung, J. I. Kim, J. Kang and B. Park, *J Power Sources*, 2012, 220, 108-113.
47. H. Zhang, Y. Wang, D. Yang, Y. Li, H. Liu, P. Liu, B. J. Wood and H. Zhao, *Advanced Materials*, 2012, 24, 1598-1603.
48. Y. Bai, Z. Xing, H. Yu, Z. Li, R. Amal and L. Wang, *ACS Applied Materials & Interfaces*, 2013, 5, 12058-12065.

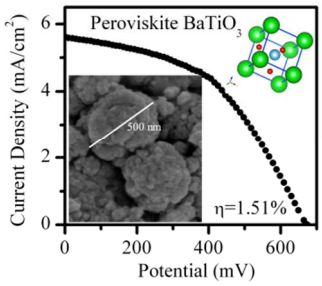

For the first time, perovskite $BaTiO_3$ nanoparticles were applied as a photoelectrode material for quantum dot sensitization in solar cells, yielding a promising power conversion efficiency of 1.51%.